THE JOURNAL OF PHYSICAL CHEMISTRY C
A JOURNAL OF THE AMERICAN CHEMICAL SOCIETY

Growth, Structure and Optical Properties of Neat, Bilayer and Codeposited Thin Films: Combining Dibenzoselenadiazoloquinoxaline with Diindenoperylene and Pentacene

Anton Pylypenko,* Dmitry Lapkin,* Elena Chulanova, Ivan Zaluzhnyy, Valentin Munteanu, Alexander Gerlach, Alexander Hinderhofer, Matthias Schwartzkopf, Maciej Jankowski, Oleg Konovalov, and Frank Schreiber*

Cite This: *J. Phys. Chem. C* 2025, 129, 21223−21234

Read Online

ACCESS | Metrics & More | Article Recommendations | Supporting Information

ABSTRACT: A crucial aspect of the fabrication of optoelectronic devices based on organic small molecules is the understanding of the growth and the postgrowth effects in thin films of these molecules. One of the factors that can negatively impact the performance of a given material despite its suitability in terms of electrical and optical properties is the dewetting of the produced film. The present work reveals the growth behavior and the postgrowth effects in thin films of dibenzoselenadiazoloquinoxaline (dbSeQ), a new organic semiconductor, thin films of which tend to dewet on Si/SiO_x substrates. To overcome this limiting feature, we deposited thin films of dbSeQ in combination with well-studied organic semiconductors, namely, diindenoperylene (DIP) and pentacene (PEN) at room and low substrate temperatures (RT and LT, respectively). Using X-ray scattering techniques, *i.e.* grazing-incidence small-angle X-ray scattering (GISAXS) and X-ray reflectivity (XRR), we characterized the growth and the annealing of thin films *in situ* in real time. The combination of atomic force microscopy (AFM), grazing-incidence wide-angle X-ray scattering (GIWAXS) and UV−Vis absorption spectroscopy provides additional important information about the morphology, structure and optical properties of the deposited films *ex situ*. We found that in thin films grown at RT, dbSeQ molecules predominantly adopt an edge-on orientation, which leads to formation of pronounced islands on the substrate. This growth mode of dbSeQ was also observed in bilayer and codeposited films with DIP and PEN. In case of LT growth, dbSeQ molecules adopt a lying orientation that in turn results in a very smooth dbSeQ layer. Further findings reveal pronounced structural and morphological changes in LT-grown films during their annealing to RT. These results are of great importance for understanding the growth of organic semiconductors incorporating fused 1,2,5-selenadiazoles and the factors that influence it, which can be used for the future development of thin film-based devices.

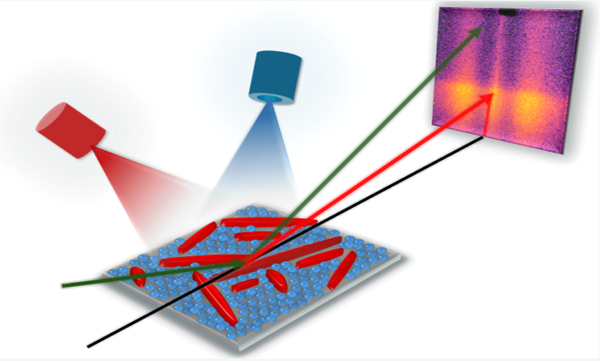

INTRODUCTION

Organic semiconductor thin films play a crucial role in various optoelectronic applications, including organic photovoltaics (OPVs), organic light-emitting diodes (OLEDs), and organic field-effect transistors (OFETs).[1−5] A key strategy to optimize the electronic properties of these devices involves controlling the molecular arrangement of donor and acceptor materials, which can be achieved through different preparation approaches. Two widely used approaches are bulk heterojunctions (BHJs), where donor and acceptor molecules are codeposited to form the active medium, and planar heterojunctions (PHJs), where distinct donor and acceptor layers are sequentially deposited.[6−13]

The performance of organic electronic devices depends on the ability to prepare thin films that are smooth, continuous, and structurally well ordered.[14,15] Many molecular semiconductors that display excellent intrinsic electronic properties, however, suffer from morphological instabilities during deposition or postgrowth. In particular, strong roughening during growth and postgrowth dewetting are challenges for the reliable preparation of high-quality thin-film devices.

Received: September 12, 2025
Revised: October 30, 2025
Accepted: November 3, 2025
Published: November 12, 2025

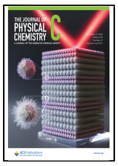

https://doi.org/10.1021/acs.jpcc.5c06408

Dewetting phenomena in molecular thin films have long been recognized as a challenge in organic thin-film fabrication and have been the subject of extensive studies.[16] Well-studied examples of postgrowth dewetting include dinaphthothienothiophene (DNTT),[17,18] α-sexithiophene (6T),[19] and diindenoperylene (DIP).[20]

The dewetting and roughening processes are mainly governed by substrate−molecule interactions and temperature. During deposition, dewetting tendencies may already manifest and intermingle with kinetic roughening processes, making it challenging to disentangle the contributions of thermodynamics and kinetics. After growth, additional reorganization can occur dependent on temperature, revealing the activation barriers associated with interfacial instabilities.

In this work, we investigate a molecular semiconductor with promising electronic characteristics, but which turns out to exhibit an unfortunate tendency to dewet. Differently substituted 1,2,5-thia- and selenadiazoles have found applications in photovoltaics and optoelectronics as electron-accepting core.[21−26] Incorporation of fused 1,2,5-thia/selenadiazoles in donor−acceptor copolymers results in increased power conversion efficiency reaching values of more than 18%.[27−29] Here, we examine the growth, resulting structure, and optical properties of neat, bilayer and codeposited thin films incorporating a novel material dibenzo[*f*,*h*][1,2,5]-selenadiazolo[3,4-*b*] quinoxaline (dbSeQ, Figure 1).[30,31] Despite its excellent electronic properties, its tendency to dewet on Si/SiO$_x$ substrates so far appears to limit its applicability in optoelectronic devices.[32]

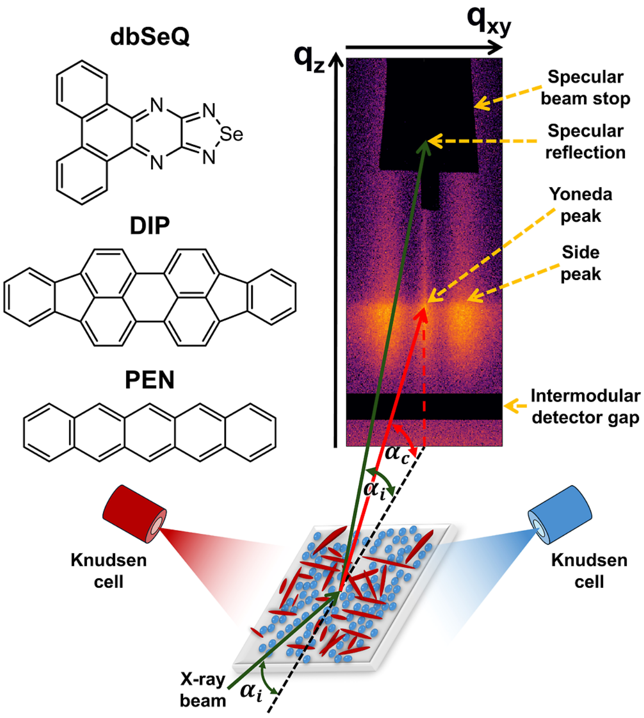

Figure 1. Chemical structures and experimental setup. Chemical structures of the small organic molecules used (left). Schematic of the experimental setup for GISAXS measurements during codeposition of two organic semiconductors (right). X-ray beam scatters with an incidence angle α_i and the critical angle of the material denotes as α_c. q_{xy} and q_z denote the horizontal and vertical components of the scattering vector, respectively.

To improve the morphology of the resulting film and create charge transfer states, we combined dbSeQ with two donor materials, diindenoperylene (DIP) and pentacene (PEN), extensively studied organic semiconductors with excellent electronic properties and high structural order.[33−41] We study both their growth and structure as well as complementary optical properties.

By comparing low-temperature (LT) growth with deposition at room temperature (RT), we probe how temperature controls the onset and strength of dewetting during film formation. Furthermore, by annealing the LT-grown films to room temperature, we study the postgrowth evolution of morphology, allowing us to extract information on the activation temperature of the dewetting transition. We examined the growth and structure of both on-top deposition and codeposition of dbSeQ with DIP and PEN. *In situ* X-ray scattering is an ideal tool to gain insights into dewetting growth process and associated thin film parameters in real-time (layer thickness, roughness, island sizes).[42] X-ray reflectivity (XRR), grazing-incidence wide-angle X-ray scattering (GIWAXS), and grazing-incidence small-angle X-ray scattering (GISAXS) provided insights into thin-film structure and growth mechanisms, while atomic force microscopy (AFM) and optical absorption spectroscopy allowed for a detailed analysis of morphological and optical properties. Our results reveal differences in the growth dynamics of dbSeQ in layered and codeposited systems, shedding light on templating effects and mixing scenarios. By comparing these findings, we establish a direct correlation between the deposition conditions, molecular interactions, and the resulting film morphology, which is crucial for the design of next-generation organic electronic devices.

■ MATERIALS AND METHODS

dbSeQ was synthesized and provided by the group of Prof. Zibarev (Novosibirsk Institute of Organic Chemistry) and used as received.[30] DIP was received purified by gradient sublimation from the University of Stuttgart, Germany. PEN was obtained from Sigma-Aldrich with a purity of 99.9% and was used without further purification. The chemical structures of the three compounds are presented in Figure 1.

Thin films were grown in a portable vacuum chamber under ultrahigh vacuum conditions using organic molecular beam deposition (OMBD).[42−45] We used two types of substrates: silicon wafers (Si(100), p-type doped) with a native oxide layer for X-ray and AFM characterization and quartz wafers for UV−Vis absorption spectroscopy. Before the deposition, we cleaned the substrates in an ultrasonic bath with acetone and isopropanol for 10 min each, followed by heating to 480 K inside the vacuum chamber for 12 h.

During film growth, the substrate temperature was maintained at 303 K (room temperature, RT) or 173 K (low temperature, LT). The deposition rate was monitored using a quartz crystal microbalance (SQM-160, Inficon). For the deposition of neat compounds, the deposition rate was 0.3 nm/min, and for codeposited compounds the total deposition rate was 0.6 nm/min.

In situ XRR scans and real-time GISAXS measurements for neat dbSeQ films and films containing DIP were performed at beamline ID10-SURF at the ESRF (Grenoble, France)[46] using an X-ray beam focused to 17 × 35 μm^2 (hor. × vert.) with a wavelength of 1.033 Å. The GISAXS measurements were conducted at an incidence angle of 0.4° (*i.e.*, above the critical

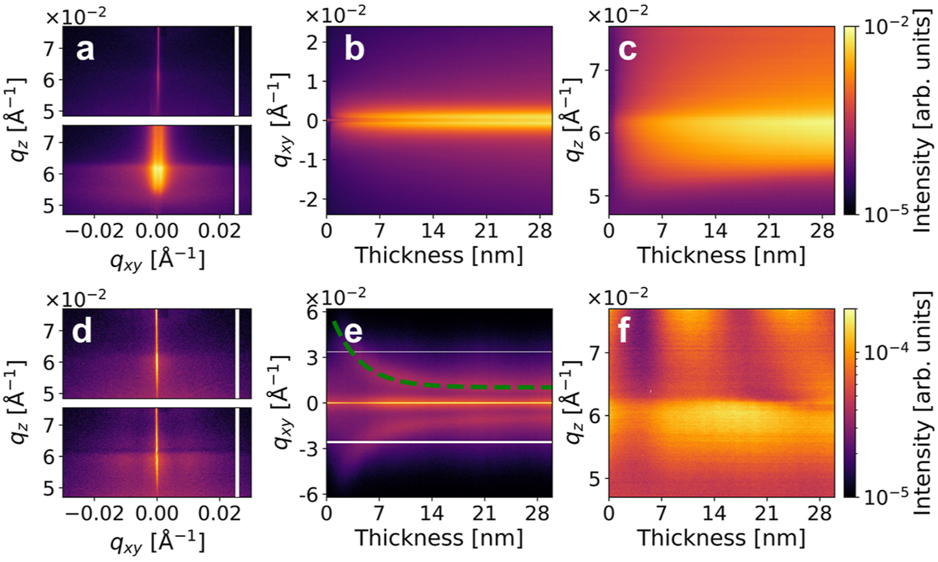

Figure 2. *In situ* GISAXS analysis of the growth of neat dbSeQ thin films (d_{nom} = 30 nm) on Si/SiO$_x$ at RT (top row, panels (a−c)) and LT (bottom row, panels (d−f)). 2D GISAXS patterns measured at the beginning (top part) and end (bottom part) of the deposition (a,d), and evolution of the intensity in the horizontal cut of the GISAXS pattern (integrated in the range of q_z = 0.056−0.060 Å^{-1}) (b,e) and vertical cut (integrated in the range of q_{xy} = −0.001−0.001 Å^{-1}) (c,f) during the deposition as a function of the thickness. The green dashed line in panel (e) shows the fit result of the side peak position. The white vertical and horizontal lines are due to intermodular gaps of the detector.

angle of the Si/SiO$_x$ substrate and all organic layers) using a 2D detector (Dectris EIGER X 4M, pixel size 75 × 75 μm^2) placed at a distance of 4000 mm from the sample.

In situ real-time GISAXS measurements for films containing PEN were performed at beamline P03 at DESY (Hamburg, Germany)[47] using an X-ray beam focused to 27 × 25 μm^2 (hor. × vert.) with a wavelength of 1.044 Å at an incidence angle of 0.4°. A 2D detector (Dectris PILATUS 2M, pixel size 172 × 172 μm^2) was used for the experiment, with a sample-to-detector distance of 4115 mm. A sketch of the experimental setup is presented in Figure 1.

All *ex situ* XRR scans were measured on a lab diffractometer (GE XRD-3003TT) using CuK$_{\alpha 1}$ radiation (λ = 1.5406 Å). *Ex situ* GIWAXS characterization was performed on a Xeuss 2.0 (Xenocs) in-house instrument using CuK$_\alpha$ radiation (λ = 1.542 Å) at an incidence angle of 0.2°, employing a PILATUS 300K detector (Dectris).

The surface morphology of the thin films was characterized *ex situ* using AFM microscopy in tapping mode, which was performed using a NanoWizard II microscope (JPK Instruments). *Ex situ* UV−Vis absorption spectra were measured in transmission mode using a PerkinElmer Lambda 950 UV−Vis−NIR spectrometer.

The AFM data was analyzed using the Gwyddion software package.[48] XRR data were fitted using the custom-developed program based on the `refnx` data analysis package[49] and the `reflectorch (mlreflect 2.0)` data analysis package that utilizes the machine learning approach.[50−52] GIWAXS data were processed using `pygid` Python data analysis package for fast data reduction.[53]

RESULTS AND DISCUSSION

Morphology Evolution during Growth. We tracked the morphology evolution of the thin films by *in situ* GISAXS measurements during their growth in real time. This technique allows a nondestructive and precise observation of the growth process and has already proved its applicability for the investigation of comparatively rough thin films of neat dbSeQ.[11,32,54−56]

We start with the case of neat dbSeQ films grown on a Si/SiO$_x$ at RT. Figure 2a shows GISAXS patterns taken at the beginning and at the end of the deposition. At the initial deposition stage, the prominent central streak at q_{xy} = 0 originating from the Si/SiO$_x$ substrate is observable. As deposition continues, two symmetrically located side peaks emerge, suggesting the formation of laterally correlated structures on the substrate.[57] The position of the side peaks corresponds to the correlation length $D_{corr} \approx 2\pi/q_{xy}$, where q_{xy} is the fitted peak position.[54] D_{corr} can be interpreted as a characteristic lateral length scale of the average electon density distribution of the features on the substrate and is affected by the interisland distance (*e.g.*, structure factor). Subsequently, these side peaks obscure the central peak, due to the increased film roughness and respective nanostructure formation.[58]

Quantitative information is extracted by making line cuts along q_{xy} (horizontal line cut) at the Yoneda peak position of dbSeQ (corresponding to $q_{z,c}$(dbSeQ) = 0.558 Å^{-1} in the current experiment) and along q_z at q_{xy} = 0 (vertical line cut). Figure 2b,c present the temporal evolution of horizontal and vertical intensity cuts, respectively, plotted *versus* the nominal thickness of the deposited film. As demonstrated in Figure 2b, as the nominal thickness approaches 1 nm, two symmetrically located peaks with respect to q_{xy} = 0 emerge and at this point D_{corr} equals 617 ± 15 nm. As the growth continues, we observe the increase in intensity of the side peaks that arises from the increase in the amount of dbSeQ on the substrate surface. During the deposition, the correlation length slightly increases and at the end of the deposition the correlation length yields D_{corr} = 795 ± 5 nm. As illustrated in Figure 2c, the temporal evolution of vertical intensity cuts reveals a pronounced Yoneda peak that becomes more intense during the deposition process. This is attributed to an increase in the amount of material illuminated by the X-ray beam. The *in situ* XRR analysis (a typical XRR curve is presented in Figure S6a in the

https://doi.org/10.1021/acs.jpcc.5c06408
J. Phys. Chem. C 2025, 129, 21223−21234

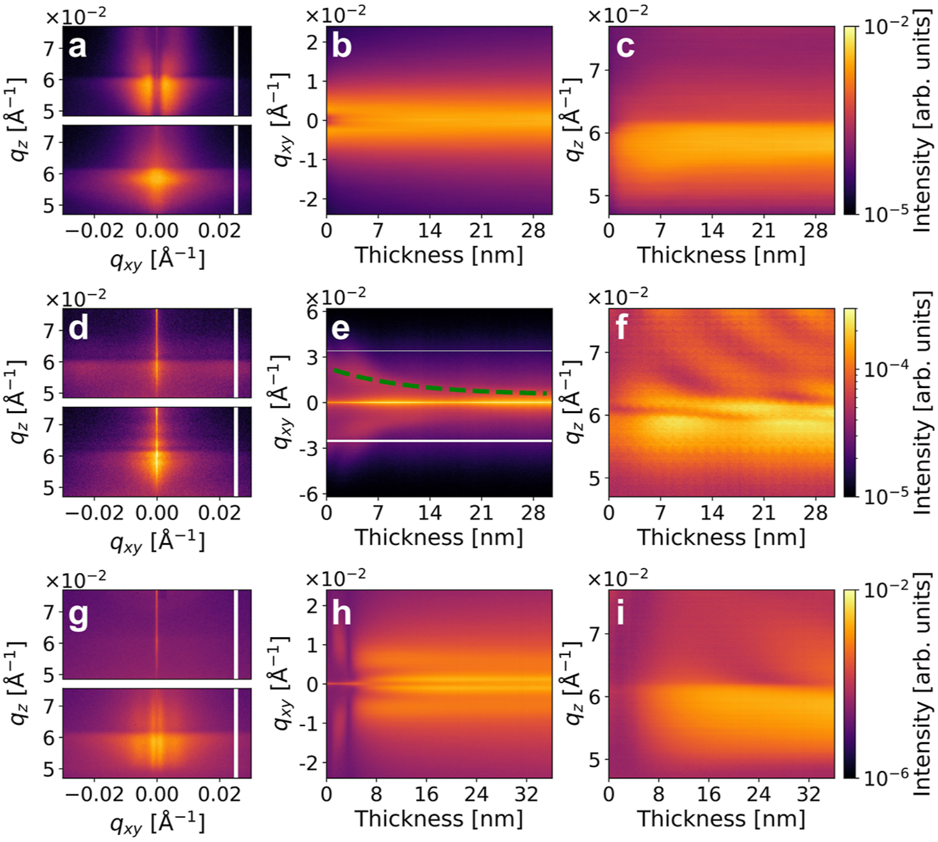

Figure 3. *In situ* GISAXS analysis of the growth of: bilayer dbSeQ/DIP thin films on Si/SiO$_x$ at RT (d_{nom}(dbSeQ) = 30 nm) (top row, panels (a–c)) and LT (d_{nom}(dbSeQ) = 30 nm) (middle row, panels (d–f)) and codeposited dbSeQ/DIP 1:1 thin film on Si/SiO$_x$ at RT (d_{nom}(total) = 36 nm) (bottom row, panels (g–i)). 2D GISAXS patterns measured at the beginning (top part) and end (bottom part) of the deposition (a,d,g), and evolution of the intensity in the horizontal cut (integrated in the range of q_z = 0.056–0.060 Å^{-1}) (b,e,h) and vertical cut (integrated in the range of q_{xy} = −0.001–0.001 Å^{-1}) (c,f,i) of the GISAXS pattern during the deposition as a function of the thickness. The green dashed line in panel (e) shows the fit result of the side peak position. The white vertical and horizontal lines are due to intermodular gaps of the detector.

Supporting Information) does not show any features because of very high surface roughness of the resulting film. We conclude that for the RT growth of neat dbSeQ, pronounced island growth is observed from the beginning of the deposition and the growth mode remains unchanged.

A comparison of the growth of neat dbSeQ at LT with its growth at RT reveals several differences. As demonstrated in Figure 2d, for the LT growth of dbSeQ, a prominent central streak that arises from Si/SiO$_x$ is observable. Throughout the entire deposition process, the central peak remains uncovered by the side peaks. This indicates a low film roughness, a finding that is confirmed by the *in situ* XRR measurements presented in the next section. Figure 2e,f present the temporal evolution of horizontal and vertical intensity cuts, respectively, plotted *versus* the nominal thickness of the deposited film. As illustrated in Figure 2e, it is possible to differentiate between two distinct stages of growth, namely 0–10 and 10–30 nm. In the initial stage at $d_{nom} \approx 3.1$ nm, the side peaks appear at relatively large q_{xy} values (q_{xy} = 0.032 Å^{-1}). These peaks undergo a rapid shift toward lower q_{xy} values indicating the nucleation and growth of the film. As the nominal film thickness reaches 10 nm, the peak position becomes almost unchanged with minimal fluctuations. The shift in the side peak position can be described by an exponential function $q_{xy}(d) = q_0 + A\exp\left(-\frac{d}{d_0}\right)$, where q_0 = 0.01 Å^{-1}, A = 0.057 Å^{-1}, and d_0 = 2.67 nm (dashed line in Figure 2e).[59] The fit is presented in Figure S1a in the Supporting Information. The corresponding correlation length D_{corr} at the beginning of the deposition (d_{nom} = 1.7 nm) equals 20 ± 1 nm, and at the end (d_{nom} = 30 nm) it is 63.0 ± 0.8 nm. Extrapolated to the onset of growth (d_{nom} = 0 nm), the fitted curve implies a correlation length of D_{corr} = 9.4 nm.

We propose that the growth of neat dbSeQ at LT is characterized by an initial formation of flat islands and proceeds as follows. At the onset of the initial stage, a high number of small islands emerge on the surface of the substrate. Then, the islands coalesce to form larger islands, as evidenced by the increase in the correlation length. In the second stage, the increase in correlation length is negligible, indicating that the film grows predominantly vertically. The temporal evolution of vertical intensity cuts presented in Figure 2f shows the intensity modulations throughout the entire deposition. They shift toward lower q_z values, as the thickness increases, indicating the continuous vertical growth of a smooth film.[54,57] During the annealing to RT the morphology of the LT-grown film changes drastically, as was confirmed by the *in situ* XRR results discussed in the next section.

To understand the influence of an organic templating layer on the growth of the dbSeQ overlayer, we studied the growth of the bilayer dbSeQ/DIP thin films. Figure 3a presents the GISAXS patterns for the growth of bilayer dbSeQ/DIP film (nominal thicknesses d_{nom}(dbSeQ) = 30 nm, d_{nom}(DIP) = 20 nm) on Si/SiO$_x$ at RT. The two pronounced intensity peaks observed at the initial stage of the deposition (Figure 3a, top part) correspond to the templating DIP layer deposited at RT, which is consistent with the known growth behavior of DIP thin films at RT.[58] As the deposition reaches its final stage (Figure 3a, bottom part), the well-defined peaks become indistinguishable due to an increase in correlation length. More information on the system can be obtained from Figure 3b,c in which the temporal evolution of horizontal and vertical intensity cuts, respectively, is presented. As illustrated in Figure 3b, data from horizontal line cuts demonstrate that at the initial growth stage, two DIP-related side peaks are present. The correlation length, $D_{\text{corr}} = 238 \pm 3$ nm, and there is no shift in q_{xy}. This indicates that there are no alterations in periodicity or morphology of the template layer.[60] As the nominal thickness of dbSeQ reaches 1 nm, the dbSeQ-related peaks become observable. Unfortunately, the peak positions are not resolvable in the experiment, which can be attributed to large correlation length of the dbSeQ islands. The vertical line cut data in Figure 3c show the minor differences compared to the growth of neat dbSeQ at RT. It is hypothesized that in a manner analogous to the case of RT growth of a neat dbSeQ film, island formation occurs from the onset of deposition. The influence of the templating layer is evident from the correlation lengths for dbSeQ that exceed the resolution achievable in the experiment, indicating larger dbSeQ islands than those for neat RT-grown dbSeQ. XRR data for the RT-grown bilayer dbSeQ/DIP film (Figure S6b in the Supporting Information) show that there are no scattering features that are characteristic of the new structures, only DIP-related features are observable after deposition and subsequent annealing, which we attribute to the limited impact of DIP on the dbSeQ layer.

Similarly to the case of neat dbSeQ, the growth of dbSeQ on the DIP layer at LT significantly differs from its growth at RT, which is confirmed by *in situ* GISAXS data for the LT growth of bilayer dbSeQ/DIP film (nominal thicknesses $d_{\text{nom}}(\text{dbSeQ}) = 30$ nm, $d_{\text{nom}}(\text{DIP}) = 20$ nm) in Figure 3d. Likewise to the growth of neat dbSeQ at LT, the central peak with highest intensity is present during the entire deposition, indicating the high smoothness of the film (which is confirmed by *in situ* XRR measurements in the following section). The temporal evolution of horizontal intensity cuts presented in Figure 3e, reveals that at the beginning of the deposition only DIP-related peaks (corresponding correlation length $D_{\text{corr}} = 28.0 \pm 0.4$ nm) are observable. As the nominal thickness of dbSeQ equals 3 nm, we could resolve the dbSeQ-related side peaks that facilitated extracting the correlation length $D_{\text{corr}} = 34.0 \pm 0.2$ nm. In the last resolvable point ($d_{\text{nom}}(\text{dbSeQ}) = 10$ nm) it equals 66 ± 5 nm. The presence of a high-intensity central peak, originating from the smooth Si/SiO$_x$ substrate and DIP layer, in combination with relatively low-intensity side peaks, made it impossible to resolve side peaks beyond this point.

The peak position evolution during dbSeQ film growth on top of DIP can again be described by an exponential function $q_{xy}(d) = q_0 + A\exp\left(-\frac{d}{d_0}\right)$, where $q_0 = 0.005$ Å^{-1}, $A = 0.018$ Å^{-1}, and $d_0 = 10.5$ nm (dashed line in Figure 3e). We can conclude that the correlation length D_{corr} in the bilayer film decays almost five times slower than the one for neat LT-grown dbSeQ. From extrapolation of the fit to the experimental data, we derived a correlation length $D_{\text{corr}} = 104$ nm for the fully grown, 30 nm thick dbSeQ film (see Figure S1b in the Supporting Information). A vertical line cut mapping in Figure 3f reveals the pronounced intensity modulations that are indicating the continuous vertical layer growth, similarly to the growth of neat dbSeQ at LT. For the LT growth of bilayer dbSeQ/DIP, we suggest that the observed growth behavior is analogous to that of the growth of neat dbSeQ at LT. However, at the initial stage, dbSeQ inherits the correlation length of the predeposited DIP layer. The evolution of the film morphology during the annealing to RT is discussed in the following.

The next step in our investigations is the codeposition of dbSeQ with DIP at RT, and 2D GISAXS patterns taken during the RT growth of the codeposited dbSeQ/DIP 1:1 film ($d_{\text{nom}}(\text{total}) = 36$ nm) are presented in Figure 3g. Initially, only a central streak is visible, and by the end of the deposition it is completely covered by side peaks because of the increased correlation length and increased roughness. We observe two sets of side peaks that belong to both compounds, dbSeQ-related peaks closer to $q_{xy} = 0$ and DIP-related peaks at larger values. In the temporal evolution of horizontal intensity cuts in Figure 3h, we observe two distinct length scales that belong to both compounds.

It is evident that the DIP- and dbSeQ-related peaks demonstrate behavior consistent with that observed for pure compounds.[56,58,61] The absence of intensity for the DIP-related peaks at $d_{\text{nom}}(\text{total}) = 4$ nm is attributed to the closed layer of the dbSeQ and DIP mixture. At RT, the growth of the neat DIP film is characterized by a transition from layer-by-layer to island growth after 3−5 monolayers.[56,62,63] Interestingly, in the codeposited film with dbSeQ, only a single closed layer is formed before the transition to island growth. The correlation length $D_{\text{corr}}(\text{DIP})$ at the beginning of the deposition ($d_{\text{nom}}(\text{total}) = 1$ nm) equals to 63.0 ± 0.5 nm. Then the growth mode of DIP carries over to the island growth scenario, as can be seen from the minor changes in peak position. The correlation length at the thickness $d_{\text{nom}}(\text{total}) = 7$ nm equals $D_{\text{corr}}(\text{DIP}) = 108 \pm 1$ nm. It stays almost constant throughout the deposition, reaching $D_{\text{corr}}(\text{DIP}) = 119.0 \pm 0.4$ nm at the end of the deposition ($d_{\text{nom}}(\text{total}) = 36$ nm).

dbSeQ exhibits a behavior analogous to that of the RT growth of a neat compound, showing island growth after the first layer is closed, without a change in the growth mode. We resolved dbSeQ-related peaks corresponding to $D_{\text{corr}}(\text{dbSeQ}) = 647 \pm 6$ nm at the thickness $d_{\text{nom}}(\text{total}) = 7$ nm, and at the end of the deposition the correlation length $D_{\text{corr}}(\text{dbSeQ})$ slightly decreased to 628 ± 4 nm. As illustrated in Figure 3i, the vertical line cut mapping exhibited only minor alterations in comparison to the growth of pristine dbSeQ at RT. Slight intensity modulations in the q_z direction point to a continuous vertical growth of the DIP layer. In the case of the codeposited dbSeQ/DIP 1:1 film, it is suggested that phase separation takes place after the first layer is closed. This corresponds well to the previously reported results on codeposition of two metals.[64] A decrease in correlation length for the dbSeQ islands is observable in comparison to the growth of neat dbSeQ. This phenomenon can be attributed to the influence of DIP in the codeposited film. Figure S6c in the Supporting Information shows the *in situ* postgrowth XRR scans of the RT-grown codeposited dbSeQ/DIP 1:1 film with a nominal thickness of 36 nm. Only the features related to the DIP are observed, including the Bragg peak at $q_z = 0.375$ Å^{-1}. The absence of dbSeQ-related features indicates the high roughness of the dbSeQ islands.

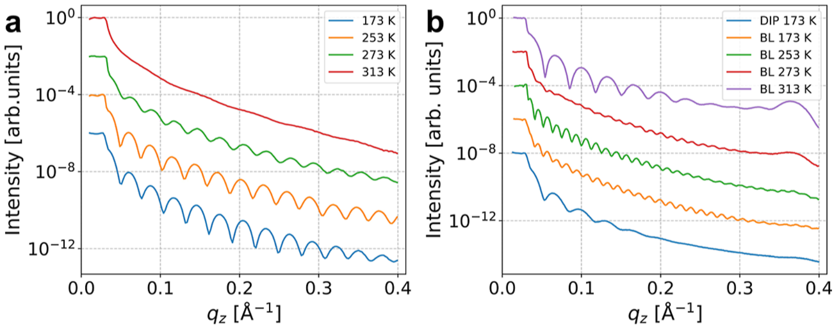

Figure 4. XRR measurements of the samples grown at LT post growth and during the annealing to RT: neat dbSeQ on Si/SiO$_x$ (a) and dbSeQ/DIP bilayer (BL) (b). All curves are vertically offset for clarity. For fitting and data analysis see Figure S7 in the Supporting Information.

Heterostructures incorporating dbSeQ and PEN show a qualitatively similar growth behavior to the structures with DIP, where the islands of dbSeQ and PEN exhibit unresolvably large correlation lengths for the bilayer and codeposited films. Moreover, we suggest, based on GISAXS, AFM and GIWAXS data, a phase separation behavior for the codeposited dbSeQ/PEN 1:1 film grown at RT, similarly to dbSeQ/DIP 1:1 at RT. The results for the bilayer dbSeQ/PEN and codeposited dbSeQ/PEN 1:1 films are presented in Figure S2a−d in the Supporting Information, respectively. The *ex situ* XRR data for the bilayer dbSeQ/PEN film and the codeposited dbSeQ/PEN 1:1 film are presented in Figure S6d in the Supporting Information, and reveal the absence of the new scattering features for these samples, where only the features from PEN are observable.

Morphology Evolution during Annealing to RT. To investigate the evolution of the morphology of the thin films grown at LT during their annealing to RT, *in situ* XRR and GISAXS measurements were performed. Figure 4a presents a postgrowth XRR scan of a neat dbSeQ film (d_{nom} = 30 nm) deposited at LT (blue curve) along with scans recorded at subsequent annealing steps up to 313 K.

Pronounced Kiessig fringes are visible for all but the scan at RT, indicating very smooth films up to this temperature. Above 273 K, the XRR results resembled those previously observed for RT-grown films (Figure S6a in the Supporting Information). This indicates that the LT-grown film is initially very smooth and remains smooth as the temperature increases, until it reaches 273 K. In the temperature region between 273 and 313 K, the film exhibits strong roughening, which leads to the absence of fringes in the XRR pattern. Fitting the data using two approaches, as shown in Figure S7a in the Supporting Information, reveals the low roughness for the dbSeQ film ($\sigma = 0.41 \pm 0.03$ nm) which persists up to 273 K. Strong roughening is attributed to the strong dewetting of the thin film as a result of an increased thermal energy. Additional GISAXS data was obtained during each annealing step and the results are presented in Figures S3 and S5a in the Supporting Information. Another consequence of the dewetting is a change in the correlation length of the neat LT-grown film with each annealing step, from $D_{\text{corr}} = 62 \pm 3$ nm at T = 173 K to $D_{\text{corr}} = 182 \pm 5$ nm at T = 313 K.

In situ XRR data for bilayer dbSeQ/DIP film (d_{nom}(dbSeQ) = 30 nm, d_{nom}(DIP) = 20 nm) grown at LT are shown in Figure 4b. DIP films grown at low temperature on Si/SiO$_x$ predominantly adopt the λ-crystalline phase with DIP molecules in lying-down geometry on the substrate and are characterized by smooth surface.[65,66] At the same time, a weak Bragg peak at approximately 0.37 Å^{-1} is observed for the postgrowth DIP XRR scan. This Bragg reflection is characteristic of the σ-phase of DIP with standing-up molecules, which is known to coexist with the λ-phase.[67−69] The roughness of the DIP layer defined from the fit of the Kiessig oscillations (Figure S7b in the Supporting Information) is 1.10 ± 0.02 nm. After dbSeQ was deposited, the roughness decreased to 0.44 ± 0.01 nm. We observe slight roughening of the film after annealing to 253 K, where the roughness of dbSeQ layer equals 0.91 ± 0.02 nm and as temperature reaches 273 K, we observe changes in contrast for the Kiessig fringes which indicate that the coverage of the dbSeQ layer has changed. Starting from T = 253 K, the Bragg reflection at $q_z \approx 0.37$ Å^{-1} becomes more pronounced as the temperature increases, which we attribute to reorientation of the DIP domains from λ- to σ-orientation. As temperature reaches 313 K, we observe the absence of the dbSeQ-related features, and the smoothening of DIP film, to the roughness of 0.40 ± 0.01 nm. We do not observe new Bragg peaks attributable to dbSeQ neither directly after its growth nor after the annealing. GISAXS data was obtained during each annealing step and the results are presented in Figures S4 and S5b in the Supporting Information. We observe a decrease in the correlation length with every annealing step up to 313 K, from $D_{\text{corr}} = 190 \pm 7$ nm at T = 253 K to $D_{\text{corr}} = 70 \pm 5$ nm at T = 273 K. Above T = 273 K, the correlation length increases to $D_{\text{corr}} = 246 \pm 4$ nm at T = 313 K, which can be attributed to the desorption of the dbSeQ molecules due to dewetting, which in turn uncovers the DIP with higher correlation length.

***Ex Situ* Morphology Studies in Real Space.** The AFM data for the neat dbSeQ films grown at RT and LT after their annealing to RT are presented in Figure 5a,b, respectively. We observe that at RT dbSeQ forms pronounced needle-like islands, randomly oriented on the substrate surface, with separate islands that reach up to 190 nm in height for a film with a nominal thickness of 24 nm. The surface coverage equals ∼40%, and the interisland distance D_{ii} equals 746 ± 245 nm, which is in good agreement with the GISAXS data, for which $D_{\text{corr}} = 795 \pm 5$ nm.

The average length of the islands is 913 ± 470 nm, and the average width is 197 ± 50 nm. The average roundness of the islands (width/length ratio) is equal to 0.28 ± 0.17, where 1 would be a perfect circle.

The AFM image of the LT-grown film of neat dbSeQ (d = 17 nm) reveals the presence of numerous randomly oriented islands that do not exhibit the same needle-like morphology as the RT-grown film. The surface coverage is a bit smaller, *i.e.* 26%, and the interisland distance is $D_{\text{ii}} = 435 \pm 159$ nm, while

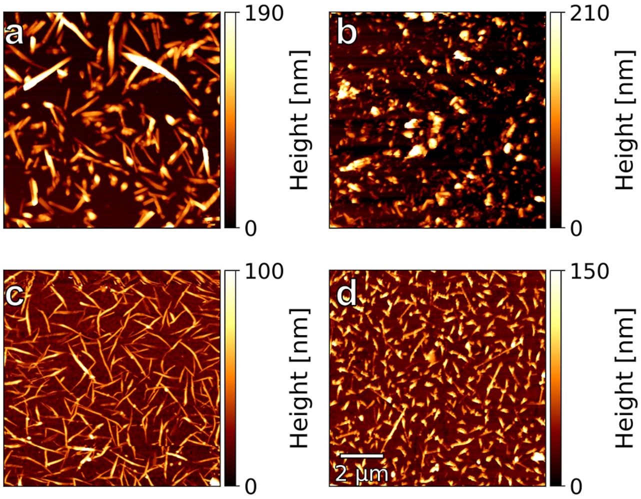

Figure 5. Real space AFM characterization of the grown films: neat dbSeQ film grown at RT (a), neat dbSeQ grown at LT (b), bilayer dbSeQ/DIP film grown at RT (c) and codeposited dbSeQ/DIP 1:1 film grown at RT (d).

the GISAXS data shows the correlation length 63.0 ± 0.8 nm for the film of comparable thickness. This discrepancy can be explained by the strong dewetting during annealing of the film to RT after growth at LT. The average length of the islands is 336 ± 143 nm and the average width is 192 ± 85 nm. The mean roundness of the islands is 0.61 ± 0.22, which is closer to the round particles than the islands appearing in the RT-grown sample.

The AFM image of the bilayer dbSeQ/DIP film (d_{dbSeQ} = 8 nm, d_{DIP} = 20 nm) grown at RT is presented in Figure 5c. The morphology of the bilayer film differs from that of the pristine dbSeQ film grown on Si/SiO$_x$, where the islands of dbSeQ in the bilayer film are more pronounced and uniform, while the surface coverage is about 33%. The interisland distance is D_{ii} = 530 ± 220 nm, while the correlation length from the GISAXS data is higher than the experimental resolution. We speculate that this is due to the overlap of the needle-like islands of dbSeQ. The average length of the islands is 881 ± 351 nm, and the average width is 116 ± 28 nm. The average roundness of the islands equals 0.21 ± 0.13, indicating that the dbSeQ islands in the bilayer film are more elongated than the islands in neat dbSeQ film.

The morphology for a RT-grown codeposited dbSeQ/DIP 1:1 film (d_{dbSeQ} = 17 nm, d_{DIP} = 25 nm) is presented in Figure 5d. The average island length equals 549 ± 316 nm and the average width equals 165 ± 35 nm, with average roundness equal to 0.33 ± 0.17, while the surface coverage is about 36%. The average interisland distance of dbSeQ D_{ii} = 556 ± 183 nm is in a good agreement with the correlation length extracted from GISAXS data that equals D_{corr} = 628 ± 4 nm. Compared to the neat dbSeQ film, the islands of dbSeQ in the codeposited film are almost 2-fold shorter, which we attribute to the sterical competition between dbSeQ and DIP islands.

The AFM data for RT-grown heterostructures that incorporate PEN are presented in Figure S8 in the Supporting Information. For the bilayer dbSeQ/PEN film we observe the overlapping elongated dbSeQ islands, as for the bilayer dbSeQ/DIP film. For the codeposited dbSeQ/PEN 1:1 film we observe the needle-like dbSeQ islands that are smaller than the ones for the bilayer film. We can clearly see the islands of PEN between the islands of dbSeQ indicating a phase-separation of both compounds in the codeposited film.

Crystalline Structure of the Films. GIWAXS patterns measured *ex situ* for various neat, bilayer and codeposited films of dbSeQ and DIP are presented in Figure 6. For the RT-grown and LT-grown films of neat dbSeQ pictured in Figure 6a,b, respectively, we observe the difference in the GIWAXS patterns caused by the reorientation of the unit cells on the substrate under the influence of substrate temperature.[32] Thin films of dbSeQ grown at RT show Debye−Scherrer rings at q = 0.50, 0.79, 0.85, 1.00, 1.34 Å^{-1} with the maximum of intensity

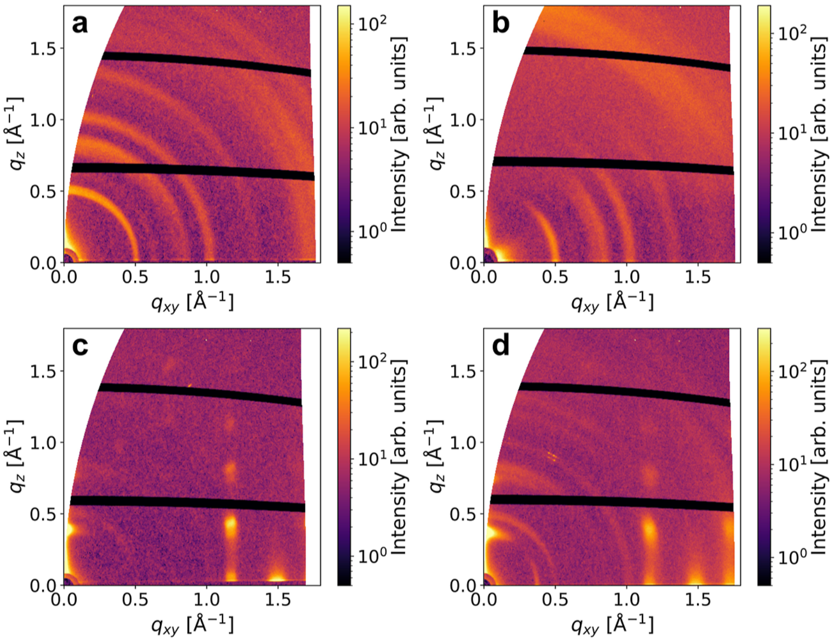

Figure 6. GIWAXS data for: neat film of dbSeQ grown at RT (a), neat film of dbSeQ grown at LT (b), bilayer film of dbSeQ/DIP grown at RT (c), codeposited film of dbSeQ/DIP 1:1 (d).

aligned along q_z and rings at $q = 1.69, 2.03, 2.26$ Å^{-1} with the maximum of intensity aligned along q_{xy}. This corresponds to the known dbSeQ structure with the unit cell parameters a = 3.88 Å, b = 15.85 Å, c = 20.33 Å, $\alpha = \gamma = 90°$, $\beta = 90.567°$ with the preferred [001] orientation (σ-phase with the edge-on orientation of molecules).

The LT-grown dbSeQ film also shows Debye−Scherrer rings at the same q-values, but compared to the RT-grown film, most of the intensity for rings at q = 0.50, 0.79, 0.85, 1.00, and 1.34 Å^{-1} is aligned along q_{xy}, and for rings at q = 1.69, 2.03, 2.26 Å^{-1} most of the intensity is aligned along q_z. This intensity realignment indicates the [100] orientation of the same unit cell corresponding to the λ-phase of the dbSeQ, where the molecules exhibit the face-on orientation.[32] Importantly, the results for the LT-grown film were obtained after annealing back to RT; therefore, these data are for the annealed film after its dewetting.

GIWAXS data for the bilayer dbSeQ/DIP film grown at RT are presented in Figure 6c. The measured patterns reveal the presence of pronounced intensity peaks, which are predominantly attributed to DIP (truncation rods at q_{xy} = 1.17 and 1.48 Å^{-1} and a bright peak at $q_{xy} = 0$, q_z = 0.37 Å^{-1}). All these peaks belong to the thin film σ-phase of DIP,[70] while the weak Debye−Scherrer rings (q = 0.50, 0.85, and 1.05 Å^{-1}) are related to dbSeQ. The absence of new features in the GIWAXS data indicates the weak influence of DIP on ordering of dbSeQ.

The results obtained for the codeposited dbSeQ/DIP 1:1 film confirm above suggestions about phase separation during codeposition. In Figure 6d we observe intense peaks of DIP (truncation rods at q_{xy} = 1.17, 1.48, 1.71 Å^{-1} and two peaks at $q_{xy} = 0$, q_z = 0.37 Å^{-1} and 0.72 Å^{-1}) and weak Debye−Scherrer rings related to dbSeQ (q = 0.50, 0.85, and 1.05 Å^{-1}). We observe the absence of new features indicative of a new mixed crystalline structure or enhanced long-range order in the codeposited film; however, there is a peak at q_{xy} = 0.37 Å^{-1}, q_z = 0 which corresponds to λ-phase of DIP, indicating the partial reorientation of DIP molecules due to the presence of dbSeQ.

GIWAXS data for heterostructures that incorporate PEN are presented in Figure S9 in the Supporting Information and show that for the bilayer dbSeQ/PEN film the most pronouncedly visible peaks belong to the thin film phase of PEN while the weak Debye−Scherrer rings arise from dbSeQ. Similarly to the bilayer dbSeQ/DIP film, we observe the absence of new features characteristic for new structure or different phases of dbSeQ, that in turn indicates the weak influence of PEN templating layer on the dbSeQ overlayer. For the codeposited dbSeQ/PEN 1:1 film, there are no new diffraction peaks indicative of a new mixed crystalline structure. However, we observe an intense peak at q_{xy} = 0.16 Å^{-1} and q_z = 0.42 Å^{-1} that corresponds to the tilted by 21° Holmes bulk phase of PEN.[71] We attribute the appearance of this phase of PEN to the influence of dbSeQ in the codeposited film.

Optical Properties. In Figure 7, we present the UV−Vis absorption spectra normalized to film thickness. For the RT-grown neat dbSeQ film we observe five absorption peaks, at 2.50, 2.85, 3.17, 3.90, and 4.89 eV. The shape of the absorption spectrum in the thin film resembles the shape of the spectrum in solution; however, the peaks are broadened and slightly red-shifted.[31]

For the LT-grown film, we observe an absorption spectrum that generally resembles that of the RT-grown film but with some differences in relative peak intensity. The position of the maximum peak remains largely unchanged, with the exception of the peak at 3.90 eV for the RT-grown film, which exhibits a slight red shift of 0.09 eV for the LT-grown film. The peak at 3.17 eV in the LT film has the highest intensity among adjacent ones, while for the RT-grown film the peak at 2.50 eV has the highest intensity. The absorption peak at 4.89 eV for the LT-grown film has much higher intensity compared to the RT-grown film. We attribute these differences to the reorientation of dbSeQ from σ-phase at RT to λ-phase at LT, as confirmed by GIWAXS.

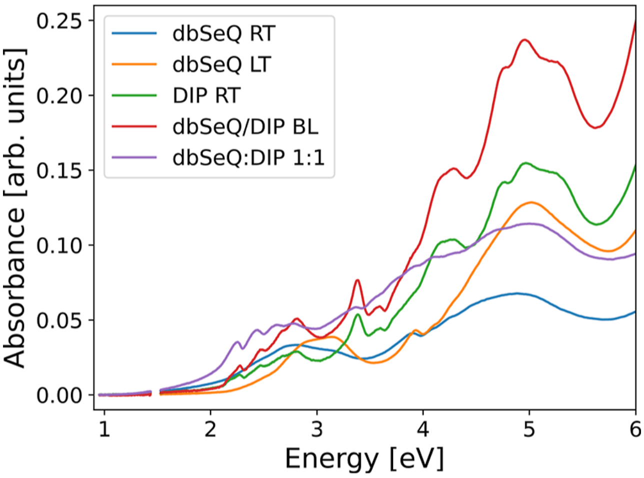

Figure 7. Optical absorption spectra in UV−Vis region for the various thin films incorporating dbSeQ and DIP, normalized to the film thickness. Gaps at about 1.5 eV originate from the switch of the detector.

The absorption spectrum of the bilayer dbSeQ/DIP film demonstrates minor discrepancies in the peak position compared to the absorption of neat DIP. The dbSeQ-related peaks in the bilayer film are practically invisible because of much greater absorption of thicker layer of DIP in the UV−Vis range. It is evident that no new peak emerges, thereby indicating the negligible influence of the DIP layer on the absorption spectrum of the bilayer film.

The absorption spectrum of the codeposited dbSeQ/DIP 1:1 film shows features of the λ-phase of DIP in the codeposited film. This is evident from the different relative intensity of the low-energy peaks (2.27, 2.47, 2.67, and 2.80 eV) compared to the RT-grown DIP film.[70] It confirms that dbSeQ in the codeposited film influences the orientation of DIP molecules with respect to the substrate, being in line with our GIWAXS results shown above. Furthermore, presence of dbSeQ in the codeposited film causes a reduction in the intensity of the peaks above 3 eV, compared to neat DIP.

The UV−Vis data for heterostructures that incorporate PEN are presented in Figure S10 in the Supporting Information. For the bilayer dbSeQ/PEN and codeposited dbSeQ/PEN 1:1 films we observe the absorption spectra that can be described as a superposition of both compounds. For the codeposited film, we observe the presence of different PEN polymorphs, which is evident from a change in relative peak intensities for peaks in the energy range of 1.5−2.6 eV.[70] We attribute this observation to the formation of tilted Holmes phase as confirmed by GIWAXS.

Table 1. Structural Parameters for Individual Films at Different Growth Stages

sample	σ (nm)	D_{corr} (nm)	D_{ii} (nm)	$\langle l \rangle$ (nm)	$\langle w \rangle$ (nm)	coverage (%)	phase
dbSeQ RT	27[a]	620 → 795	746	913	197	40	σ
dbSeQ LT	0.4	20 → 63	n/a	n/a	n/a	n/a	λ
dbSeQ LT at RT	42[a]	182	435	336	192	26	λ
dbSeQ/DIP RT	3	>238	530	881	116	33	σ
dbSeQ/DIP LT	0.5	34 → 66	n/a	n/a	n/a	n/a	n/a
dbSeQ/DIP LT at RT	0.4[c]	246[c]	n/a	n/a	n/a	n/a	n/a
dbSeQ/DIP RT	3	647 → 628[b] 63 → 119[c]	556	549	165	36	σ[b] λ, σ[c]
dbSeQ/PEN RT	14[a]	349 → 731	706	1020	219	31	σ
dbSeQ/PEN RT	17[a]	>456[d]	476	661	180	32	σ[b] λ, σ[d]

[a] Values derived from AFM analysis. [b] dbSeQ. [c] DIP. [d] PEN.

■ SUMMARY AND CONCLUSION

In summary, the present study has explored the growth, structure, and optical properties of neat dbSeQ and its blends with DIP and PEN in different heterostructures. We studied the growth of these systems at LT and observed the strong dewetting of the LT-grown films during their annealing to RT. The results are summarized in Table 1 in which the structural parameters for the initial and later growth stages, and the annealing stage, are presented.

It was found that dbSeQ on Si/SiO$_x$ at RT grows in the form of rough, randomly oriented, needle-shaped, long crystallites. The correlation distances obtained by GISAXS and AFM are in the sub-μm range. dbSeQ crystallizes predominantly in the σ-phase, where the molecules are standing with a tilted edge-on configuration. The absorption spectrum in the UV−Vis range exhibits five distinct peaks and resembles the one measured in solution.

Conversely, the growth of dbSeQ at LT is characterized by significantly smaller correlation lengths and lower roughness, compared to the RT-grown film, which we attribute to the change in the molecular orientation of dbSeQ. It was observed that the low thermal stability of the LT-grown dbSeQ films resulted in strong dewetting during their annealing to RT. This, in turn, resulted in high roughness of the resulting film. The resulting islands are generally smaller and more circular than that observed for the RT-grown film. From the GIWAXS results, it is evident that the crystallites are oriented in the λ-phase in contrast to the σ-phase formed during growth at RT. This change in the molecular orientation leads to alterations in the absorption spectrum, resulting in a variation in the relative intensity of the peaks, as was previously found for different organic films grown at RT and LT.[70]

The growth of dbSeQ on top of a DIP film at RT results in large, rough, needle-like islands of dbSeQ with a correlation length exceeding the experimental resolution. Compared to a neat dbSeQ film, the crystallites of dbSeQ grown on DIP are more elongated. From the AFM data, we found that the correlation length is so large because of the overlap of the islands of dbSeQ. Additional characterization by XRR, GIWAXS, and absorbance spectroscopy did not show signs of a different crystalline nor electronic structure.

The growth of dbSeQ on top of the DIP film at LT has several differences compared to the growth of neat dbSeQ. At the beginning, the correlation length of dbSeQ is equal to that of DIP, which means that dbSeQ grows in the gaps between DIP islands. After the initial stage, a subsequent fast increase in the correlation length beyond the resolution limit of the experiment is observed. Notably, the decay of the correlation length of dbSeQ in the bilayer is almost five times slower than that for the neat compound. From the XRR it is evident that the layer of dbSeQ on DIP has a low roughness that remains stable until annealing to 273 K. Above this temperature, we observed only DIP-related scattering features as a result of the strong dewetting of the dbSeQ film. Interestingly, the dbSeQ layer does not prevent DIP from the bottom layer from reorientation to its σ-phase during annealing of the film to RT.

The growth of coevaporated dbSeQ/DIP 1:1 film at RT is characterized by mixing of both compounds in the first monolayer. After the first layer is closed, a phase separation growth scenario occurs. In the codeposited film, the dbSeQ islands are shorter and exhibit more circular shape in comparison to those observed in the neat dbSeQ film at RT. We found that the interisland distances for dbSeQ in the codeposited film are smaller compared to the growth of neat dbSeQ at RT. Interestingly, the presence of dbSeQ in the codeposited film allows DIP to form only one closed monolayer, instead of 3−5 monolayers, as was previously found for neat DIP. Sterical competition of the islands of both compounds results in shorter dbSeQ islands compared to those of neat dbSeQ. Additionally, we observe the presence of the λ-phase of DIP molecules in the codeposited film which can be also attributed to the influence of dbSeQ.

For the growth of dbSeQ on PEN at RT, we observe the same growth behavior as for the bilayer dbSeQ/DIP film, where the correlation length of dbSeQ is large and rapidly exceeds the experimental resolution. From the AFM data, we observe the large overlapping islands of dbSeQ. We do not observe the influence of the PEN layer on the optical or structural properties of dbSeQ.

The growth of the codeposited dbSeQ/PEN 1:1 film at RT is characterized by large interisland distances beyond the experimental resolution for both compounds. We observe a growth pattern that resembles the one for codeposited dbSeQ/DIP 1:1 film. We suggest that, likewise to the codeposited film with DIP, the codeposited film with PEN exhibits a phase-separation growth scenario. From absorption spectroscopy and GIWAXS, we found that for the codeposited film a tilted Holmes bulk phase of PEN appeared.

We demonstrate the growth behavior of dbSeQ in various heterostructures and how it can be influenced by the substrate temperature. The general trend for the growth of neat and bilayer films at RT is formation of long, rod-shaped islands of dbSeQ, with interisland distances in the sub-μm range. Neat and bilayer films deposited at LT form a smooth layer during growth, with correlation lengths order of magnitude smaller than those for RT-growth. The annealing of these films to RT leads to strong dewetting, which in turn results in strong roughening of the films, indicating the limited thermal stability of the LT-grown films. Simultaneous deposition of two materials at RT leads to a clear phase separation in the resulting films, but for the codeposited film with DIP we suggest that a mixing occurs in the first monolayer. The islands of dbSeQ are generally smaller in the codeposited films than those of neat dbSeQ, because of the sterical competition of the islands of both compounds. Additionally, it was found that the presence of dbSeQ in codeposited films leads to the appearance of a different phase of the second compound. Our results provide crucial insight into the understanding of growth mechanisms in donor−acceptor blends, which could be used for the development of device architectures. We expect that despite this work showing results for combinations of dbSeQ with two mostly studied organic semiconductor materials, the scenarios mentioned above are applicable to other rod-shaped OSCs. The search for other binary mixtures that can enhance the thermal stability and structural order of films with dbSeQ is underway.

■ ASSOCIATED CONTENT

Supporting Information

The Supporting Information is available free of charge at https://pubs.acs.org/doi/10.1021/acs.jpcc.5c06408.

> Additional experimental details, fit procedures, additional GISAXS, XRR, GIWAXS, AFM and UV−Vis data for heterostructures with PEN are available in Supporting Information (PDF)

■ AUTHOR INFORMATION

Corresponding Authors

Anton Pylypenko − *Institut für Angewandte Physik, Universität Tübingen, 72076 Tübingen, Germany*; orcid.org/0009-0000-6510-3818; Email: anton.pylypenko@uni-tuebingen.de

Dmitry Lapkin − *Institut für Angewandte Physik, Universität Tübingen, 72076 Tübingen, Germany*; Email: dmitry.lapkin@uni-tuebingen.de

Frank Schreiber − *Institut für Angewandte Physik, Universität Tübingen, 72076 Tübingen, Germany; Center for Light-Matter Interaction, Sensors and Analytics LISA+, Universität Tübingen, 72076 Tübingen, Germany*; orcid.org/0000-0003-3659-6718; Email: frank.schreiber@uni-tuebingen.de

Authors

Elena Chulanova − *Institut für Angewandte Physik, Universität Tübingen, 72076 Tübingen, Germany*; orcid.org/0000-0001-5452-6831

Ivan Zaluzhnyy − *Institut für Angewandte Physik, Universität Tübingen, 72076 Tübingen, Germany*; orcid.org/0000-0001-5946-2777

Valentin Munteanu − *Institut für Angewandte Physik, Universität Tübingen, 72076 Tübingen, Germany*

Alexander Gerlach − *Institut für Angewandte Physik, Universität Tübingen, 72076 Tübingen, Germany*; orcid.org/0000-0003-1787-1868

Alexander Hinderhofer − *Institut für Angewandte Physik, Universität Tübingen, 72076 Tübingen, Germany*; orcid.org/0000-0001-8152-6386

Matthias Schwartzkopf − *Deutsches Elektronen-Synchrotron DESY, 22607 Hamburg, Germany*; orcid.org/0000-0002-2115-9286

Maciej Jankowski − *ESRF—The European Synchrotron, 38043 Grenoble, France*

Oleg Konovalov − *ESRF—The European Synchrotron, 38043 Grenoble, France*

Complete contact information is available at: https://pubs.acs.org/10.1021/acs.jpcc.5c06408

Notes

The authors declare no competing financial interest.

■ ACKNOWLEDGMENTS

The project is partially funded by the Federal Ministry of Education and Research (BMBF) and the Baden-Württemberg Ministry of Science as part of the Excellence Strategy of the German Federal and State Governments. The authors acknowledge financial support by the German Research Foundation (DFG). We acknowledge the ESRF for the provision of synchrotron facilities at beamline ID10-SURF. Furthermore, part of this research was conducted at the P03 beamline of PETRA III at DESY, a member of the Helmholtz Association (HGF). The authors thank the LISA + facility at the University of Tübingen for support.

■ REFERENCES

(1) Leman, D.; Kelly, M. A.; Ness, S.; Engmann, S.; Herzing, A.; Snyder, C.; Ro, H. W.; Kline, R. J.; DeLongchamp, D. M.; Richter, L. J. In Situ Characterization of Polymer−Fullerene Bilayer Stability. *Macromolecules* **2015**, *48*, 383−392.

(2) Chwang, A. B.; Kwong, R. C.; Brown, J. J. Graded mixed-layer organic light-emitting devices. *Appl. Phys. Lett.* **2002**, *80*, 725−727.

(3) Smith, J.; Hamilton, R.; McCulloch, I.; Stingelin-Stutzmann, N.; Heeney, M.; Bradley, D. D. C.; Anthopoulos, T. D. Solution-processed organic transistors based on semiconducting blends. *J. Mater. Chem.* **2010**, *20*, 2562.

(4) Newman, C. R.; Frisbie, C. D.; da Silva Filho, D. A.; Brédas, J.-L.; Ewbank, P. C.; Mann, K. R. Introduction to Organic Thin Film Transistors and Design of n-Channel Organic Semiconductors. *Chem. Mater.* **2004**, *16*, 4436−4451.

(5) Hains, A. W.; Liang, Z.; Woodhouse, M. A.; Gregg, B. A. Molecular Semiconductors in Organic Photovoltaic Cells. *Chem. Rev.* **2010**, *110*, 6689−6735.

(6) Crone, B. K.; Davids, P. S.; Campbell, I. H.; Smith, D. L. Device model investigation of bilayer organic light emitting diodes. *J. Appl. Phys.* **2000**, *87*, 1974−1982.

(7) Duva, G.; Beyer, P.; Scholz, R.; Belova, V.; Opitz, A.; Hinderhofer, A.; Gerlach, A.; Schreiber, F. Ground-state charge-transfer interactions in donor:acceptor pairs of organic semiconductors − a spectroscopic study of two representative systems. *Phys. Chem. Chem. Phys.* **2019**, *21*, 17190−17199.

(8) Qiu, L.; Lim, J. A.; Wang, X.; Lee, W. H.; Hwang, M.; Cho, K. Versatile Use of Vertical-Phase-Separation-Induced Bilayer Structures in Organic Thin-Film Transistors. *Adv. Mater.* **2008**, *20*, 1141−1145.

(9) Zhang, D.; Zhong, W.; Ying, L.; Fan, B.; Li, M.; Gan, Z.; Zeng, Z.; Chen, D.; Li, N.; Huang, F.; et al. Overcoming incompatibility of donors and acceptors by constructing planar heterojunction organic solar cells. *Nano Energy* **2021**, *85*, 105957.

(10) Li, Y.; Lin, Y. Planar heterojunctions for reduced non-radiative open-circuit voltage loss and enhanced stability of organic solar cells. *J. Mater. Chem. C* **2021**, *9*, 11715−11721.

(11) Banerjee, R.; Novák, J.; Frank, C.; Lorch, C.; Hinderhofer, A.; Gerlach, A.; Schreiber, F. Evidence for Kinetically Limited Thickness Dependent Phase Separation in Organic Thin Film Blends. *Phys. Rev. Lett.* **2013**, *110*, 185506.

(12) Hinderhofer, A.; Gerlach, A.; Kowarik, S.; Zontone, F.; Krug, J.; Schreiber, F. Smoothing and coherent structure formation in organic-organic heterostructure growth. *Europhys. Lett.* **2010**, *91*, 56002.

(13) Brütting, W. *Physics of Organic Semiconductors*; John Wiley & Sons, Ltd, 2005; pp 1−14.

(14) Opitz, A.; Duva, G.; Gebhardt, M.; Kim, H.; Meister, E.; Meisel, T.; Beyer, P.; Belova, V.; Kasper, C.; Pflaum, J.; et al. Thin films of electron donor−acceptor complexes: characterisation of mixed-crystalline phases and implications for electrical doping. *Mater. Adv.* **2022**, *3*, 1017−1034.

(15) Peumans, P.; Uchida, S.; Forrest, S. R. Efficient bulk heterojunction photovoltaic cells using small-molecular-weight organic thin films. *Nature* **2003**, *425*, 158−162.

(16) Burke, S. A.; Topple, J. M.; Grütter, P. Molecular dewetting on insulators. *J. Phys.: Condens. Matter* **2009**, *21*, 423101.

(17) Breuer, T.; Karthäuser, A.; Klemm, H.; Genuzio, F.; Peschel, G.; Fuhrich, A.; Schmidt, T.; Witte, G. Exceptional Dewetting of Organic Semiconductor Films: The Case of Dinaphthothienothiophene (DNTT) at Dielectric Interfaces. *ACS Appl. Mater. Interfaces* **2017**, *9*, 8384−8392.

(18) Acharya, R.; Günder, D.; Breuer, T.; Schmitz, G.; Klauk, H.; Witte, G. Stability of organic thin-film transistors based on ultrathin films of dinaphtho[2,3-b:2′,3′-f]thieno[3,2-b]thiophene (DNTT). *J. Mater. Chem. C* **2021**, *9*, 270−280.

(19) Albonetti, C.; Barbalinardo, M.; Milita, S.; Cavallini, M.; Liscio, F.; Moulin, J.-F.; Biscarini, F. Selective Growth of α-Sexithiophene by Using Silicon Oxides Patterns. *Int. J. Mol. Sci.* **2011**, *12*, 5719−5735.

(20) Kowarik, S.; Gerlach, A.; Sellner, S.; Cavalcanti, L.; Schreiber, F. Dewetting of an Organic Semiconductor Thin Film Observed in Real-time. *Adv. Eng. Mater.* **2009**, *11*, 291−294.

(21) Xia, D.; Wang, X.-Y.; Guo, X.; Baumgarten, M.; Li, M.; Müllen, K. Fused Bis-Benzothiadiazoles as Electron Acceptors. *Cryst. Growth Des.* **2016**, *16*, 7124−7129.

(22) Cortizo-Lacalle, D.; Gozalvez, C.; Olano, M.; Sun, X.; Melle-Franco, M.; Hueso, L. E.; Mateo-Alonso, A. Bisthiadiazole-Fused Tetraazapentacenequinone: An Air-Stable Solution-Processable n-Type Organic Semiconductor. *Org. Lett.* **2015**, *17*, 5902−5905.

(23) Gu, P.-Y.; Zhang, J.; Long, G.; Wang, Z.; Zhang, Q. Solution-processable thiadiazoloquinoxaline-based donor−acceptor small molecules for thin-film transistors. *J. Mater. Chem. C* **2016**, *4*, 3809−3814.

(24) Jung, J. W.; Jo, J. W.; Jung, E. H.; Jo, W. H. Recent progress in high efficiency polymer solar cells by rational design and energy level tuning of low bandgap copolymers with various electron-withdrawing units. *Org. Electron.* **2016**, *31*, 149−170.

(25) Neto, B. A. D.; Lapis, A. A. M.; da Silva Júnior, E. N.; Dupont, J. 2,1,3-Benzothiadiazole and Derivatives: Synthesis, Properties, Reactions, and Applications in Light Technology of Small Molecules. *Eur. J. Org Chem.* **2013**, *2013*, 228−255.

(26) Mori, H. Development of semiconducting polymers based on a novel heteropolycyclic aromatic framework. *Polym. J.* **2021**, *53*, 975−987.

(27) Liu, Q.; Jiang, Y.; Jin, K.; Qin, J.; Xu, J.; Li, W.; Xiong, J.; Liu, J.; Xiao, Z.; Sun, K.; et al. 18% Efficiency organic solar cells. *Sci. Bull.* **2020**, *65*, 272−275.

(28) Nie, Q.; Tang, A.; Guo, Q.; Zhou, E. Benzothiadiazole-based non-fullerene acceptors. *Nano Energy* **2021**, *87*, 106174.

(29) Jin, K.; Xiao, Z.; Ding, L. D18, an eximious solar polymer. *J. Semicond.* **2021**, *42*, 010502.

(30) Konstantinova, L. S.; Bobkova, I. E.; Nelyubina, Y. V.; Chulanova, E. A.; Irtegova, I. G.; Vasilieva, N. V.; Camacho, P. S.; Ashbrook, S. E.; Hua, G.; Slawin, A. M. Z.; et al. [1, 2, 5]Selenadiazolo[3, 4-b]pyrazines: Synthesis from 3, 4-Diamino-1, 2, 5-selenadiazole and Generation of Persistent Radical Anions. *Eur. J. Org Chem.* **2015**, *2015*, 5585−5593.

(31) Radiush, E. A.; Korshunov, V. M.; Chulanova, E. A.; Konstantinova, L. S.; Ferulev, A. I.; Irtegova, I. G.; Shundrina, I. K.; Frank, E. A.; Semenov, N. A.; Taidakov, I. V.; et al. Polycyclic 1,2,5-chalcogenadiazole dyes: structural, optical, and redox properties in neutral and radical-ion states (chalcogen = S, Se). *Dyes Pigments* **2025**, *242*, 112922.

(32) Pylypenko, A.; Chulanova, E.; Unger, F.; Keck, J.; Zaluzhnyy, I.; Dax, I.; Schwartzkopf, M.; Gerlach, A.; Hinderhofer, A.; Meixner, A. J.; Schreiber, F. Thin Films of Conjugated Chalcogenadiazole: Growth, Structure, and Optical Properties of Substituted Selenadiazoloquinoxaline. *J. Phys. Chem. C* **2024**, *128*, 8104−8113.

(33) Dürr, A. C.; Koch, N.; Kelsch, M.; Rühm, A.; Ghijsen, J.; Johnson, R. L.; Pireaux, J.-J.; Schwartz, J.; Schreiber, F.; Dosch, H.; et al. Interplay between morphology, structure, and electronic properties at diindenoperylene-gold interfaces. *Phys. Rev. B* **2003**, *68*, 115428.

(34) Dürr, A. C.; Schreiber, F.; Ritley, K. A.; Kruppa, V.; Krug, J.; Dosch, H.; Struth, B. Rapid Roughening in Thin Film Growth of an Organic Semiconductor (Diindenoperylene). *Phys. Rev. Lett.* **2003**, *90*, 016104.

(35) Wagner, J.; Gruber, M.; Hinderhofer, A.; Wilke, A.; Bröker, B.; Frisch, J.; Amsalem, P.; Vollmer, A.; Opitz, A.; Koch, N.; et al. High Fill Factor and Open Circuit Voltage in Organic Photovoltaic Cells with Diindenoperylene as Donor Material. *Adv. Funct. Mater.* **2010**, *20*, 4295−4303.

(36) Hinderhofer, A.; Schreiber, F. Organic−Organic Heterostructures: Concepts and Applications. *ChemPhysChem* **2012**, *13*, 628−643.

(37) Wilson, M. W.; Rao, A.; Ehrler, B.; Friend, R. H. Singlet exciton fission in polycrystalline pentacene: from photophysics toward devices. *Acc. Chem. Res.* **2013**, *46*, 1330−1338.

(38) Kitamura, M.; Arakawa, Y. Pentacene-based organic field-effect transistors. *J. Phys.: Condens. Matter* **2008**, *20*, 184011.

(39) Kowarik, S.; Gerlach, A.; Leitenberger, W.; Hu, J.; Witte, G.; Wöll, C.; Pietsch, U.; Schreiber, F. Energy-dispersive X-ray reflectivity and GID for real-time growth studies of pentacene thin films. *Thin Solid Films* **2007**, *515*, 5606.

(40) Dax, I.; Zaluzhnyy, I. A.; Pylypenko, A.; Russegger, N.; Starostin, V.; Rysov, R.; Westermeier, F.; Sprung, M.; Hinderhofer, A.; Pithan, L.; et al. Insight into heterogeneous dynamics of growing islands using coherent x-ray scattering. *New J. Phys.* **2023**, *25*, 103033.

(41) Lapkin, D.; Nasro, R.; Hagara, J.; Hofferberth, B.; Hinderhofer, A.; Gerlach, A.; Schreiber, F. Vacuum chamber for deposition of gradient thin films: Toward high-throughput structure−property correlative studies. *Rev. Sci. Instrum.* **2025**, *96*, 053905.

(42) Kowarik, S.; Gerlach, A.; Schreiber, F. Organic molecular beam deposition: fundamentals, growth dynamics, and in situ studies. *J. Phys. Condens. Matter* **2008**, *20*, 184005.

(43) Forrest, S. R. Ultrathin Organic Films Grown by Organic Molecular Beam Deposition and Related Techniques. *Chem. Rev.* **1997**, *97*, 1793.

(44) Schreiber, F. Organic molecular beam deposition: Growth studies beyond the first monolayer. *Phys. Status Solidi A* **2004**, *201*, 1037.

(45) Ritley, K. A.; Krause, B.; Schreiber, F.; Dosch, H. A portable ultrahigh vacuum organic molecular beam deposition system for in situ x-ray diffraction measurements. *Rev. Sci. Instrum.* **2001**, *72*, 1453.

(46) Chulanova, E.; Dax, I.; Pylypenko, A.; Unger, F.; Zaluzhnyy, I. *Investigating the Relationship Between Photophysics and Structural Properties in Mixed Films of pi-Extended Selenadiazole [Dataset]*; European Synchrotron Radiation Facility, 2026..

(47) Buffet, A.; Rothkirch, A.; Döhrmann, R.; Körstgens, V.; Abul Kashem, M. M.; Perlich, J.; Herzog, G.; Schwartzkopf, M.; Gehrke, R.; Müller-Buschbaum, P.; et al. P03, the microfocus and nanofocus X-ray scattering (MiNaXS) beamline of the PETRA III storage ring: the microfocus endstation. *J. Synchrotron Radiat.* **2012**, *19*, 647−653.

(48) Nečas, D.; Klapetek, P. Gwyddion: an open-source software for SPM data analysis. *Cent. Eur. J. Phys.* **2012**, *10*, 181.

(49) Nelson, A. R. J.; Prescott, S. W. *refnx*: neutron and X-ray reflectometry analysis in Python. *J. Appl. Crystallogr.* **2019**, *52*, 193–200.

(50) Greco, A.; Starostin, V.; Edel, E.; Munteanu, V.; Rußegger, N.; Dax, I.; Shen, C.; Bertram, F.; Hinderhofer, A.; Gerlach, A.; et al. Neural network analysis of neutron and X-ray reflectivity data: automated analysis using mLreflect, experimental errors and feature engineering. *J. Appl. Crystallogr.* **2022**, *55*, 362.

(51) Hinderhofer, A.; Greco, A.; Starostin, V.; Munteanu, V.; Pithan, L.; Gerlach, A.; Schreiber, F. Machine learning for scattering data: strategies, perspectives and applications to surface scattering. *J. Appl. Crystallogr.* **2023**, *56*, 3–11.

(52) Munteanu, V.; Starostin, V.; Greco, A.; Pithan, L.; Gerlach, A.; Hinderhofer, A.; Kowarik, S.; Schreiber, F. Neural network analysis of neutron and X-ray reflectivity data incorporating prior knowledge. *J. Appl. Crystallogr.* **2024**, *57*, 456–469.

(53) Abukaev, A.; Völter, C.; Romodin, M.; Schwartzkopff, S.; Bertram, F.; Konovalov, O.; Hinderhofer, A.; Lapkin, D.; Schreiber, F. A Python Package for Fast Data Reduction in Grazing-Incidence Diffraction (GID). *J. Appl. Crystallogr.* **2025**, submitted.

(54) Schwartzkopf, M.; Buffet, A.; Körstgens, V.; Metwalli, E.; Schlage, K.; Benecke, G.; Perlich, J.; Rawolle, M.; Rothkirch, A.; Heidmann, B.; et al. From atoms to layers: in situ gold cluster growth kinetics during sputter deposition. *Nanoscale* **2013**, *5*, 5053.

(55) Schwartzkopf, M.; et al. Real-time insight into nanostructure evolution during the rapid formation of ultra-thin gold layers on polymers. *Nanoscale Horiz.* **2021**, *6*, 132–138.

(56) Frank, C.; Novák, J.; Banerjee, R.; Gerlach, A.; Schreiber, F.; Vorobiev, A.; Kowarik, S. Island size evolution and molecular diffusion during growth of organic thin films followed by time-resolved specular and off-specular scattering. *Phys. Rev. B* **2014**, *90*, 045410.

(57) Santoro, G.; Yu, S.; Schwartzkopf, M.; Zhang, P.; Koyiloth Vayalil, S.; Risch, J. F. H.; Rübhausen, M. A.; Hernández, M.; Domingo, C.; Roth, S. V. Silver substrates for surface enhanced Raman scattering: Correlation between nanostructure and Raman scattering enhancement. *Appl. Phys. Lett.* **2014**, *104*, 243107.

(58) Frank, C.; Banerjee, R.; Oettel, M.; Gerlach, A.; Novák, J.; Santoro, G.; Schreiber, F. Analysis of island shape evolution from diffuse x-ray scattering of organic thin films and implications for growth. *Phys. Rev. B* **2014**, *90*, 205401.

(59) Schwartzkopf, M.; Santoro, G.; Brett, C. J.; Rothkirch, A.; Polonskyi, O.; Hinz, A.; Metwalli, E.; Yao, Y.; Strunskus, T.; Faupel, F.; et al. al Real-Time Monitoring of Morphology and Optical Properties during Sputter Deposition for Tailoring Metal–Polymer Interfaces. *ACS Appl. Mater. Interfaces* **2015**, *7*, 13547–13556.

(60) Gensch, M.; Schwartzkopf, M.; Ohm, W.; Brett, C. J.; Pandit, P.; Vayalil, S. K.; Bießmann, L.; Kreuzer, L. P.; Drewes, J.; Polonskyi, O.; Strunskus, T.; et al. Correlating Nanostructure, Optical and Electronic Properties of Nanogranular Silver Layers during Polymer-Template-Assisted Sputter Deposition. *ACS Appl. Mater. Interfaces* **2019**, *11*, 29416–29426.

(61) Lorch, C.; Novák, J.; Banerjee, R.; Weimer, S.; Dieterle, J.; Frank, C.; Hinderhofer, A.; Gerlach, A.; Carla, F.; Schreiber, F. Influence of C60 co-deposition on the growth kinetics of diindenoperylene–From rapid roughening to layer-by-layer growth in blended organic films. *J. Chem. Phys.* **2017**, *146*, 052807.

(62) Zhang, X.; Barrena, E.; de Oteyza, D.; Dosch, H. Transition from layer-by-layer to rapid roughening in the growth of DIP on SiO2. *Surf. Sci.* **2007**, *601*, 2420–2425.

(63) Barrena, E.; de Oteyza, D. G.; Sellner, S.; Dosch, H.; Ossó, J. O.; Struth, B. In Situ Study of the Growth of Nanodots in Organic Heteroepitaxy. *Phys. Rev. Lett.* **2006**, *97*, 076102.

(64) Schwartzkopf, M.; et al. In Situ Monitoring of Scale Effects on Phase Selection and Plasmonic Shifts during the Growth of AgCu Alloy Nanostructures for Anticounterfeiting Applications. *ACS Appl. Nano Mater.* **2022**, *5*, 3832–3842.

(65) Hinderhofer, A.; Hosokai, T.; Yonezawa, K.; Gerlach, A.; Kato, K.; Broch, K.; Frank, C.; Novák, J.; Kera, S.; Ueno, N.; et al. Post-growth surface smoothing of thin films of diindenoperylene. *Appl. Phys. Lett.* **2012**, *101*, 033307.

(66) Kowarik, S.; Gerlach, A.; Sellner, S.; Cavalcanti, L.; Konovalov, O.; Schreiber, F. Real-time X-ray diffraction measurements of structural dynamics and polymorphism in diindenoperylene growth. *Appl. Phys. A: Mater. Sci. Process.* **2009**, *95*, 233–239.

(67) Kowarik, S.; Gerlach, A.; Sellner, S.; Schreiber, F.; Cavalcanti, L.; Konovalov, O. Real-Time Observation of Structural and Orientational Transitions during Growth of Organic Thin Films. *Phys. Rev. Lett.* **2006**, *96*, 125504.

(68) Dürr, A.; Nickel, B.; Sharma, V.; Täffner, U.; Dosch, H. Observation of competing modes in the growth of diindenoperylene on SiO_2. *Thin Solid Films* **2006**, *503*, 127–132.

(69) Elsässer, P.; Schilling, T. Structural transition in the single layer growth of diindenoperylene on silica. *J. Chem. Phys.* **2024**, *161*, 094903.

(70) Duva, G.; Mann, A.; Pithan, L.; Beyer, P.; Hagenlocher, J.; Gerlach, A.; Hinderhofer, A.; Schreiber, F. Template-Free Orientation Selection of Rod-Like Molecular Semiconductors in Polycrystalline Films. *J. Phys. Chem. Lett.* **2019**, *10*, 1031–1036.

(71) Pachmajer, S.; Jones, A. O.; Truger, M.; Röthel, C.; Salzmann, I.; Werzer, O.; Resel, R. Self-limited growth in pentacene thin films. *ACS Appl. Mater. Interfaces* **2017**, *9*, 11977–11984.